Dynamics in pattern-forming systems

H. Guo
Centre for the Physics of Materials, Rutherford Building, McGill University, 3600 rue Université, Montréal, Québec, Canada H3A 2T8 and Department of Physics, Rutherford Building, McGill University, 3600 rue Université, Montréal, Québec, Canada H3A 2T8

D. C. Hong
Department of Physics, Center for Polymer Science & Engineering, Lehigh University, Bethlehem, Pennsylvania 18015 and Center for Polymer Science & Engineering, Lehigh University, Bethlehem, Pennsylvania 18015

D. A. Kurtze
Department of Physics, North Dakota State University, Fargo, North Dakota 58105
(Received 1 November 1991)

We study the time evolution of the initial instability toward the final steady state for two pattern-forming systems: explosive crystallization and the viscous-fingering problem. We show analytically that a scaling solution exists for the power spectrum of the interface shape in the case of explosive crystallization. The scaling exponents are computed exactly. For the viscous-fingering problem, a similar scaling solution is obtained, and the scaling exponents are determined numerically. We also study the robustness of the scaling solutions against external perturbations. We find that local perturbation on the surface tension does not alter the scaling exponents, although it has dramatic influence on the late-stage steady-state patterns.

PACS number(s): 68.35.Fx, 82.65.Dp, 05.70.Ln

I. INTRODUCTION

The formation and evolution of dynamic structures is one of the most exciting areas of nonlinear phenomenology. Pattern-formation problems are common in various fields such as hydrodynamics, metallurgy, and combustion. The best studied pattern-formation problems involve growing interfaces between two phases: two solids, two fluids, or a solid and a fluid. Specific systems that have received much attention over the past several years include viscous fingering in a Hele-Shaw cell [1, 2], dendritic growth of a solid from a melt [2–4], directional solidification [3], and explosive crystallization [5–7]. All of these systems have the feature that there exists a moving boundary between two phases, on which competing stabilizing and destabilizing forces act. It is the interplay between these forces that controls the dynamical evolution of the complex patterns.

The viscous-fingering problem in a linear Hele-Shaw cell is one of the simplest examples of a wide class of nonlinear pattern-forming systems. Here an instability on the interface between two fluids sets in when a less viscous fluid pushes a more viscous one. Subsequently, a finger-shaped interfacial pattern develops. If the system is driven continually, it eventually reaches a steady state with one finger left, which is characterized by a well-defined finger width. This final state is independent of the initial conditions and is solely a function of one dimensionless parameter (see below). Similar behavior has been observed in other nonlinear systems: notable examples are dendritic solidification and explosive crystallization where the final steady states are also characterized by well-defined interfacial shapes. In all of these systems, much attention has focused on how to identify the final steady state via a selection mechanism. For viscous fingering, one believes that dynamically selected finger widths are precisely those for which steady-state solutions exist and they are determined by the solvability condition [2, 4, 8]. For explosive crystallization, selection of the final state is controlled by a continuum Lotka-Volterra equation [9, 6]. While we seem to understand these pattern-forming systems in the initial [10] and final time regimes [2, 4], much less attention is paid to the dynamics that occurs between the two regimes [11]. In the journey toward the final steady state, how does the initial instability on the interface amplify and drive the system toward the final state? How can one properly characterize the dynamic process of this intermediate regime?

In fact, the question of interfacial dynamics at the intermediate time regime has only been put into focus very recently by Jasnow and Viñals [12]. They studied the dynamical evolution of viscous fingers using a boundary integral method. Through a large-scale numerical computation, they discovered a time regime where the evolution of the pattern is self-similar; i.e., a scaling of the power spectrum of the interface shape exists. This is important since it provided a basis of the concept of dynamic universality class in the pattern-forming systems. The purpose of this paper is to further study this time regime. First, we shall show analytically that a self-similar solution indeed exists in a somewhat simpler pattern-formation problem, namely, explosive crystallization. In this case the scaling exponents can be calculated exactly. Thus the existence of dynamic scaling in the intermediate time

regime is not limited to Hele-Shaw flow. We find this to be an important step because it provides a rigorous basis for the Jasnow-Viñals scaling solutions and possibly for further renormalization-group analysis. Second, after confirming the results obtained by Jasnow and Viñals on the viscous fingering problem, we examine the robustness of the scaling solution to external perturbations, using a numerical method similar to that of Refs. [12, 13]. It has been found experimentally [14] and theoretically [15] that the late-stage pattern shape is sensitive to local perturbations since it changes the solvability condition. Thus a study such as ours may help one to understand how the mathematically quite subtle solvability mechanism, which is believed to provide the pattern-selection mechanism in this system [2, 4], comes about. As in Ref. [12], this involves a large numerical computation that is common in dealing with the generalized Stephan problem.

The paper is organized as follows. In the next section we show the existence of a scaling solution for the dynamic equation of the growing crystal front in explosive crystallization. In Sec. III we present results for the Hele-Shaw flow problem. Section IV is for a summary.

II. EXPLOSIVE CRYSTALLIZATION

The process of explosive crystallization has been discussed extensively in the literature [5–7]. Here a thin amorphous film is crystallized by locally injecting energy with, for example, a laser pulse. The latent heat that is released during the crystallization may further crystallize nearby amorphous material. Under favorable conditions, a self-sustained process occurs until the entire film crystallizes. If the initial film and substrate temperature is lower than some critical temperature, the latent heat is not enough to keep crystallization continuing, and usually one injects energy continuously to maintain the process [16]. We shall be concerned with this latter case, i.e., driven explosive crystallization. We are interested in the time evolution of the interface between the crystalline and amorphous materials.

Figure 1 sketches the system. The amorphous film is heated by a straight-line heater, such as a strip heater, which moves in the x direction with a fixed speed v. Both the source and the latent heat that is being released at the crystallization front contribute to the activation energy,

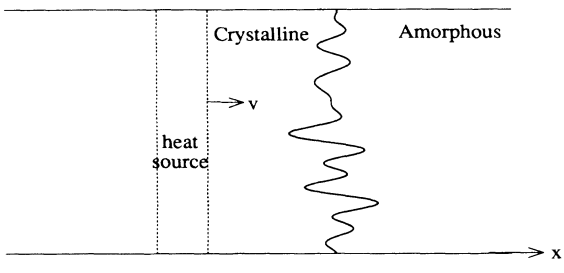

FIG. 1. Sketch of the driven explosive crystallization system. Region I is the amorphous material and region II is the crystallized material. The interface separating the two phases is moving in the x direction. A strip heater is also shown that moves with a speed v.

which causes new material to crystallize. The process can be modeled by a two-dimensional diffusion equation for the temperature of the film, including linear heat loss to the environment, and latent heat release at the interface and the source [6, 9]. The equation can then be transformed into a nonlinear equation for the interface shape. If $A(q,t)$ is the amplitude of mode q of the Fourier transform of the interface shape at time t, we define the power spectrum [12] to be $S(q,t) \equiv |A(q,t)|^2$. It has been shown that $S(q,t)$ satisfies a continuum Lotka-Volterra equation [9]

$$\frac{\partial S(q,t)}{\partial t} = \left[\Sigma(q) - \int_{-\infty}^{\infty} f(q,k)S(k,t)\,dk\right] S(q,t) \quad , \tag{1}$$

where $\Sigma(q)$ is the real part of the linear growth rate of mode q and $f(q,k)$ is a nonsymmetric function depending on system parameters, which has the reflection property $f(-q,-k) = f(q,k)$.

Instead of integrating this equation numerically, as was done in Ref. [9], we now seek a scaling solution of the form proposed by Jasnow and Viñals,

$$S(q,t) = (q-q_0)^{-\alpha} G(t(q-q_0)^z) = t^{\beta} H(t^{\frac{1}{z}}(q-q_0)) \quad , \tag{2}$$

with $\beta \equiv \alpha/z$. The exponent β describes the growth of the fastest-growing mode $q_0 = q_0(t)$ and z gives a time scale for approaching a steady state. We expect this solution to be valid in the large-time limit.

To obtain the exponent α, consider the first moment $M(t)$:

$$M(t) = \int S(q,t)\,dq \quad . \tag{3}$$

From (1) we obtain the equation of motion for $M(t)$,

$$\frac{dM(t)}{dt} = \int \Sigma(q)S(q,t)\,dq - \int\int f(q,k)S(q,t)S(k,t)\,dq\,dk \quad . \tag{4}$$

A numerical integration of Eq. (1) showed that $S(q,t)$ is sharply peaked at q_0 at large times [9]. Thus the right-hand side of (4) can be approximated and we obtain

$$\frac{dM(t)}{dt} \approx [\Sigma(q_0) - M(t)f(q_0,q_0)]M(t) \quad . \tag{5}$$

Since a steady-state pattern is selected [9] as $t \to \infty$, we have $q_0(t) \to q_\infty = \text{const}$ in that limit. Hence, asymptotically, $M(t) \to \Sigma(q_\infty)/\{f(q_\infty,q_\infty) + \exp[-\Sigma(q_\infty)t]\} \sim \text{const}$. On the other hand, substituting (2) into (3), we obtain

$$M(t) = t^{\frac{\alpha}{z}} \int H(t^{\frac{1}{z}}(q-q_0))\,dq = t^{\frac{\alpha-1}{z}} \int H(x)\,dx \quad . \tag{6}$$

In order for $M(t)$ to approach a constant in the large-time limit, we must have $\alpha = 1$.

To determine the exponent z, we study a quantity $W(t)$ which essentially is the width of the peak of $S(q,t)$,

$$W^{-2}(t) \equiv -\frac{1}{S(q,t)}\frac{\partial^2 S(q,t)}{\partial q^2}\bigg|_{q=q_0} \quad . \tag{7}$$

Since $\frac{\partial S}{\partial t}$ vanishes at the peak $q = q_0$, we easily find

$$\frac{d}{dt}W^{-2}(t) = -\frac{\partial^2}{\partial q^2}\left(\frac{1}{S}\frac{\partial S}{\partial t}\right)\bigg|_{q_0} - \frac{dq_0}{dt}\frac{\partial}{\partial q}\left(\frac{1}{S}\frac{\partial^2 S}{\partial q^2}\right)\bigg|_{q_0} \quad . \tag{8}$$

The second term is vanishingly small at large times because of the factor dq_0/dt. The first term, on the other hand, approaches a constant in the same limit. We obtain

$$W^{-2}(t) \sim -\frac{H''(0)}{H(0)}\, t^{\frac{2}{z}} \sim t \quad .$$

Thus $z = 2$. The quantity $1/W(t)$ has a natural interpretation in position space: an initially localized perturbation on the crystallization front gives rise to a patterned region on the front, whose extent is of order $1/W(t)$, because $W(t)$ is the width of the power spectrum. Now, the fact that $z = 2$ implies that this region grows diffusively for large t, i.e., $1/W(t) \approx t^{1/2}$. Recall now Parseval's theorem, which states that $\int S(q,t)dq = \int |f(x,t)|^2 dx$, where $f(x,t)$ is the front position at x and t. Since $M(t) = \int S(q,t)dq$ approaches a constant, the squared deviation of the front from its steady-state position also integrates to a constant. This, combined with the fact that the width of the front grows as $t^{1/2}$, implies that the rms displacement decays slowly, as $t^{-1/4}$.

Finally, the asymptotic form of the peak position of the power spectrum, $q_0(t)$, can also be determined. Note that $\frac{\partial S}{\partial q}|_{q_0} = 0$. Differentiating this with respect to time, we find

$$\frac{1}{W^2}\frac{dq_0}{dt} = -\frac{\partial}{\partial q}\left(\frac{1}{S}\frac{\partial S}{\partial t}\right)\bigg|_{q_0} \quad . \tag{9}$$

The right-hand side vanishes at $q = q_\infty$, since the expression is what defines q_∞. So, for q_0 near q_∞, we have

$$\frac{\partial}{\partial q}\left(\frac{1}{S}\frac{\partial S}{\partial t}\right)\bigg|_{q_0} \approx \frac{\partial^2}{\partial q^2}\left(\frac{1}{S}\frac{\partial S}{\partial t}\right)\bigg|_{q_0}(q_0 - q_\infty) \quad . \tag{10}$$

From Eqs. (8), (9), and (10), we obtain

$$q_0(t) = q_\infty + \frac{C}{t} \quad , \tag{11}$$

where C is a constant.

Given the fact that a steady-state pattern is indeed selected in driven explosive crystallization [9], we have thus shown that a scaling solution exists for the power spectrum of the interface shape which separates the crystalline and amorphous materials. Presumably it is possible to carry out a similar analysis for the viscous-fingering problem, although we have not yet done so. Instead, we shall carry out a numerical solution of the governing equations to confirm the results of Ref. [12]. In addition, we shall show that the scaling solution is quite robust against local perturbations to such quantities as the surface tension. To that we now turn.

III. VISCOUS FINGERING

When a less viscous fluid is pushing a more viscous one, the interface is unstable against long-wavelength fluctuations. As a consequence, the less viscous fluid penetrates the more viscous one in a fingerlike shape. A standard setup of the phenomenon is in a linear Hele-Shaw cell, which consists of two parallel rectangular glass plates with a small distance b in between. Initially, many fingers evolve and compete to grow; thus a coarsening process occurs. Due to the screening of the Laplacian field, larger fingers grow faster and smaller ones get left behind. At very large times, a steady-state is reached with only one finger left in the cell and its width λ is usually larger than half the channel width w. This is a representative phenomenon in a larger problem of pattern selection. Only recently has it become possible to predict the steady-state finger width and its tip velocity as a function of the external control parameter [2,4]. It has been shown that the surface tension between the two fluids plays a singular role, in that it is associated with the highest derivative of the interfacial dynamical equation [2,4]. Thus a small change in the surface tension may have a dramatic influence on the steady-state pattern. Indeed, both theory and simulation [15] have shown that if the surface tension is slightly reduced at the finger tip, the steady-state finger will have $\lambda < \frac{1}{2}w$. This is also observed [14] experimentally.

It is interesting to study the dynamics before the steady state is reached. Experimentally such a regime has been investigated by Curtis and Maher [17]. We shall use a numerical technique similar to that of Jasnow and Viñals [12,18]. We start by writing down the governing equation for the flow inside a linear Hele-Shaw cell [19] which is oriented along the y direction. For incompressible fluids the divergence of the velocity vanishes, so that the pressure field P satisfies the Laplace equation,

$$\nabla^2 P = 0 \quad . \tag{12}$$

At the interface, the standard boundary conditions on the pressure field are used,

$$v_i = -\frac{b^2}{12\mu_i}\nabla P_i \quad , \tag{13}$$

$$P_1 - P_2 = -\gamma\kappa \quad , \tag{14}$$

where v_i is the normal velocity of the fluid i at the interface, b is the thickness of the Hele-Shaw cell, μ_i is the viscosity, and γ is the surface tension. κ is the curvature, which is taken as positive if the center of the radius of the curvature lies in the pushing fluid. We consider the case where fluid 1 is pushing fluid 2 with a rate Uwb^2

per second. Then to the far right of the interface, the velocity of fluid 2 is uniform and is given by U. That is,

$$P_2 \rightarrow -\frac{12\mu_2}{b^2}Uy \quad \text{as} \quad y \rightarrow \infty \quad . \tag{15}$$

Finally, at the side walls, the normal velocity of the fluid v_n should vanish. Defining a potential $\Phi \equiv \phi + Uy$ with $\phi \equiv b^2P/12\mu$, $Y \equiv y - Ut$, and assuming $\mu_1 \approx 0$, Eqs. (13)–(15) can be rewritten as

$$\begin{aligned} v_n' &= -\hat{\mathbf{n}} \cdot \boldsymbol{\nabla}\Phi = -v_n + U\cos\theta \quad , \\ \Phi_s &= \phi_s + Uy = -\gamma\kappa + U\zeta(x) \quad , \\ \Phi &\rightarrow 0 \quad \text{as} \quad Y \rightarrow \infty \quad , \\ \left.\frac{\partial\Phi}{\partial n}\right|_{\text{wall}} &= 0 \quad , \end{aligned} \tag{16}$$

where θ is the angle between the interface normal and the $+y$ direction and $\zeta(x)$ is the y coordinate of the interface, i.e., it is the interface shape.

The last set of equations can be further reduced into an equation for the interface shape via Green's theorem. There are many ways to find the two-dimensional Green's function for our problem, which satisfies $\nabla^2 G(\mathbf{r}, \mathbf{r}') = -\delta(\mathbf{r} - \mathbf{r}')$ and is periodic in the x direction. A simple method is given in Ref. [20] and we quote the result here,

$$G(x - x', y - y') = -\frac{|y - y'|}{2w} - \frac{1}{4\pi}\ln\left[1 - 2p\cos\left(\frac{2\pi(x - x')}{w}\right) + p^2\right] \quad , \tag{17}$$

where $p = \exp(-2\pi|y - y'|/w)$. Applying Green's theorem on a contour shown in Fig. 2, we obtain

$$-\frac{1}{2}\left(\gamma\kappa(s) - \frac{U}{2}\zeta(s)\right) + \int ds'\left(\gamma\kappa(s') - \frac{U}{2}\zeta(s')\right)\frac{\partial G(s, s')}{\partial n'} = \int ds' G(s, s')v_n'(s') \quad , \tag{18}$$

where s, s' are contour variables along the interface and the integrations extend over the entire interface. Some subtleties in deriving the last equation were discussed in Ref. [12]. From this equation, we obtain the normal velocity of the interface v_n if the interface shape $\zeta(x)$ is known. The interface is then moved forward in time by essentially solving $d\zeta/dt = v_n\cos\theta$. Thus given an initial interface shape, its time evolution can be obtained.

Equation (18) is a Fredholm integral equation of the first kind, which is very difficult to tackle numerically [21]. We have used a discretization scheme discussed in the book of Jaswon and Symm [22]. The interface is parametrized by the contour variable s_i and the angle between the normal and the y direction, θ_i, at each node i. The singular contribution from $G(s, s' \rightarrow s)$ is treated using the method of Refs. [12, 20]. After the equation is discretized, the Green's-function matrix on the right-hand side of (18) is inverted to give v_n at each node. It is important to dynamically add new nodes when the curvature gets large [12]. Typically we started with $N = 150$ nodes and it could be increased up to 800 at the end of a run. To ensure stability of the solution, it is vital to make sure that the linear solution is produced accurately when $\zeta(x)$ is small [23]. Indeed, we find that the numerically obtained linear stability dispersion relation coincides with that predicted by the theory with an error bar of a few percent for the worst case, except for high wave numbers, which correspond to linearly stable modes. This is understandable since short-wavelength modes (large-wave-number) are more numerically problematic to deal with, but they do not contribute to the instability.

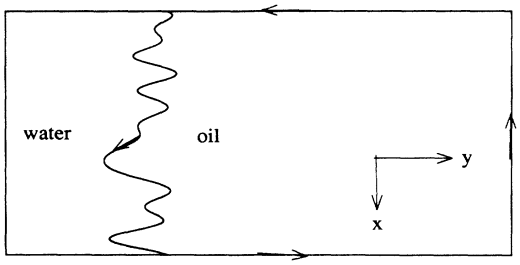

FIG. 2. Closed contour over which Green's theorem is applied to obtain Eq. (18) for the viscous-fingering problem. The fingers are growing in the y direction.

After finding v_n for each node, we advance the interface using the following kinematic equations [24, 12]:

$$\frac{\partial\theta_i}{\partial t} = \kappa(s_i)v_t(s_i) + \left.\frac{\partial v_n(s)}{\partial s}\right|_{s=s_i} \quad , \tag{19}$$

$$\frac{dS_T}{dt} = -\int_0^{S_T} ds'\ \kappa(s')v_n(s') \quad , \tag{20}$$

where

$$\begin{aligned} v_t(s) &= sg(S_T) - S_T g(s) \quad , \\ g(s) &= \frac{1}{S_T}\int_0^s ds'\ \kappa(s')v_n(s') \quad . \end{aligned}$$

The interface nodes are always equally spaced along the perimeter. Finally, as a reference point, we advance the first node ($x = 0$) explicitly using

$$\frac{\partial\zeta(s_1)}{\partial t} = v_n(s_1)\cos\theta_1 \quad . \tag{21}$$

The $N + 2$ equations of (19), (20), and (21) are then solved simultaneously using an Adams-Moulton method.

The initial interface shape is taken as a sum of the first 10 to 15 modes of sine curves with small random

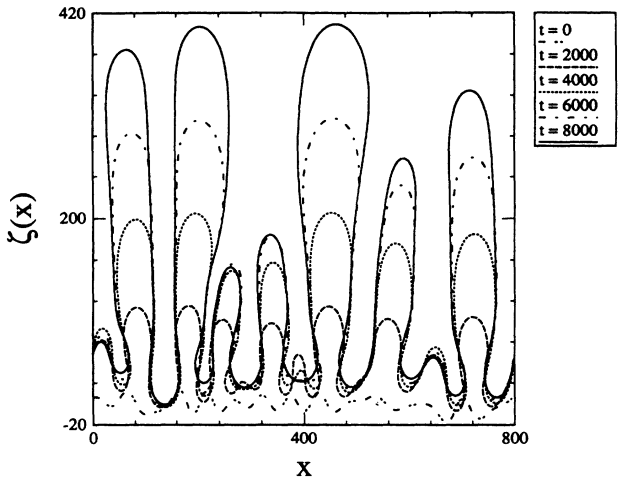

FIG. 3. Time evolution of the interface. The initial curve consists first 15 modes of sine waves with small random amplitudes. The interfaces shown here are at times $t = 0$, 4000, and 8000. Other parameters are $\gamma = 1.0$, $U = 0.025$, and $w = 800$.

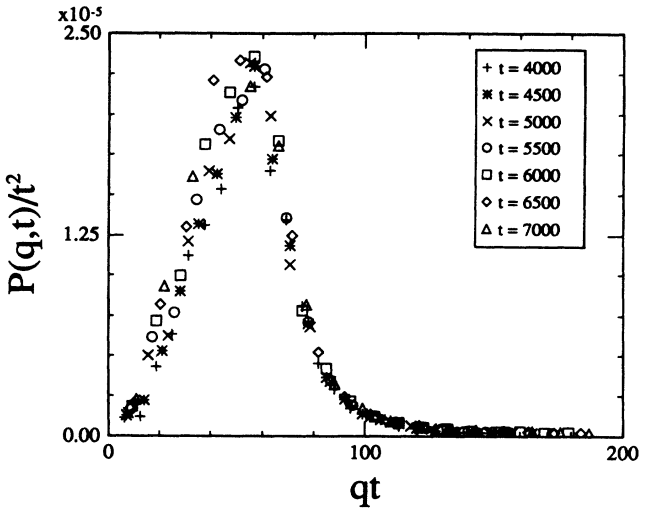

FIG. 5. Scaling plot of the data of Fig. 4, using Eq. (23). The data collapse reasonably well onto one curve. The data are a result of averaging 280 independent runs.

amplitudes. As typical parameters, we take $\gamma = 1.0$, $U = 0.025$, and $w = 600$ or 800. In Fig. 3 we show typical evolutions of the interface up to time 8000. It is evident that coarsening occurs in that smaller fingers are swallowed by larger ones. We have checked [25] that the fingers eventually collapse into one at very long times. In order to study the dynamics systematically, we consider the power spectrum of the interface shape defined by

$$P(q,t) \equiv \left\langle N^{-2}\left|\sum_{i=1}^{N} \zeta(x_i,t)e^{iqx_i}\right|^2 \right\rangle \quad , \qquad (22)$$

where the $< \cdots >$ denotes averaging over initial conditions. Figure 4 shows $P(q,t)$ as a function of q for several times t after averaging 280 independent runs. At late times the peak of $P(q,t)$ moves down to smaller values of q, indicating the coarsening process. Figure 5 checks a scaling form [12] of $P(q,t)$ similar to Eq. (2):

$$P(q,t) = t^2 F(qt) \quad . \qquad (23)$$

Indeed, the data of Fig. 4 reasonably collapse onto a single curve, indicating the scaling form of the power spectrum. This confirms the findings of Ref. [12].

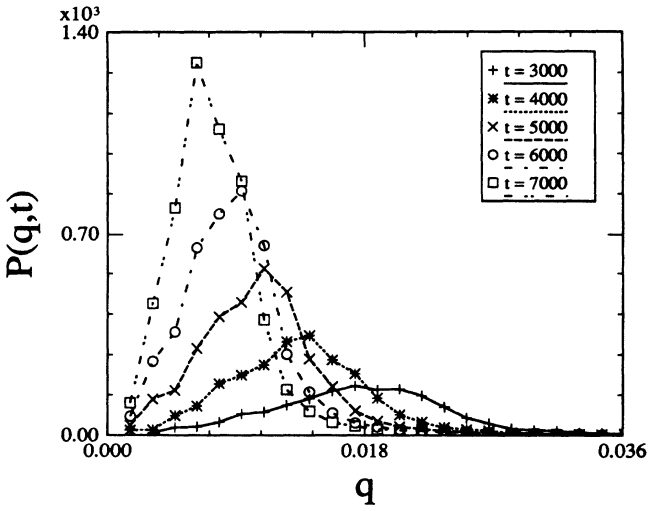

FIG. 4. Power spectrum of the interface shape $P(q,t)$ for several times t. The peak shifts down to smaller values of q, indicating a coarsening process. Other parameters are the same as those in Fig. 3.

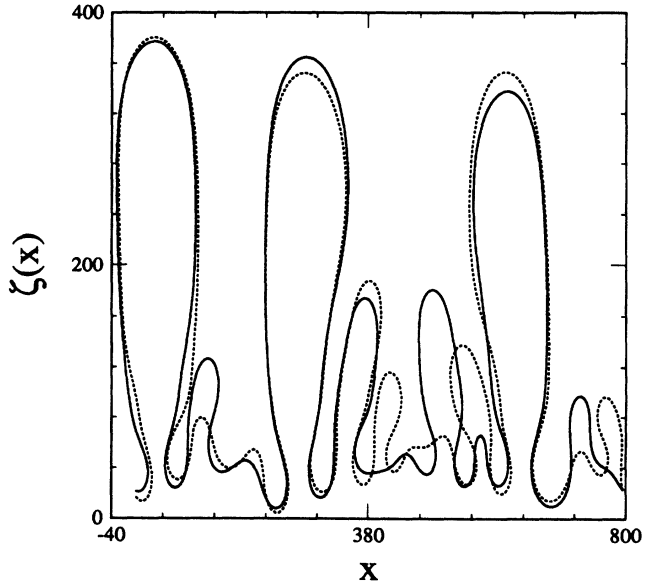

FIG. 6. Interface shapes at time $t = 7000$. The solid line is for the case with surface tension perturbation parameter $\epsilon = 0.4$ [see Eq. (24)]. The dotted curve is with $\epsilon = 0$ but otherwise with the same parameters as those used to produce the solid curve. Other parameters are the same as those of Fig. 3.

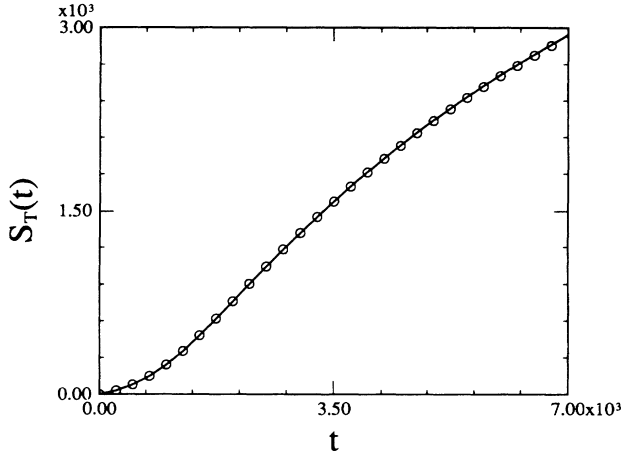

FIG. 7. Total perimeter length as a function of time for $\epsilon = 0.4$ (solid line) and $\epsilon = 0.0$ (circles). Other parameters are the same as those of Fig. 3.

As mentioned above, the surface tension of the interface plays a singular role in the steady-state pattern selection. Locally perturbing the surface tension has dramatic effects on the selected pattern [14, 15]. We now examine what effect, if any, it has on the transient dynamics. In particular, we choose to perturb the surface tension in the following way:

$$\gamma = \gamma_0 \left[1 - \epsilon \cos\left(\frac{2\pi n x}{w}\right)\right] , \tag{24}$$

where γ_0 is a constant and n is an integer. In the following we fix $\gamma_0 = 1.0$ and $n = 4$ without losing any generality [26]. This form of the perturbation might mimic the effect of putting several parallel wires into the Hele-Shaw cell. Figure 6 shows the interface shape with $\epsilon = 0$ and 0.4. It is interesting to note that the fingers alternately grow faster and slower for the $\epsilon \neq 0$ case. Figure 7 shows the total perimeter length as a function of time. Figure 8 shows the width of the interface defined as the root-mean-square value of $\zeta(x)$. As shown, there is no significant difference between the $\epsilon = 0$ and $\neq 0$ cases for these quantities. The width of the interface shows a linear dependence on time at late times, similar to that of the $\epsilon = 0$ case [12]. In Fig. 9 the scaling function of (23) is plotted for $\epsilon = 0.2$ and 0.4. This is a result of averaging 280 independent runs. Very similar behavior was also found for other values of ϵ. We may conclude that the scaling form of the power spectrum is robust against this type of perturbation on the surface tension, although there are some quantitative changes on the nonuniversal constants. This may be understood from experiences on far-from-equilibrium phenomena: short-length-scale behavior is usually not important to the dynamics. Indeed, the surface tension provides the smallest length scale in the viscous-fingering problem. We thus expect that the

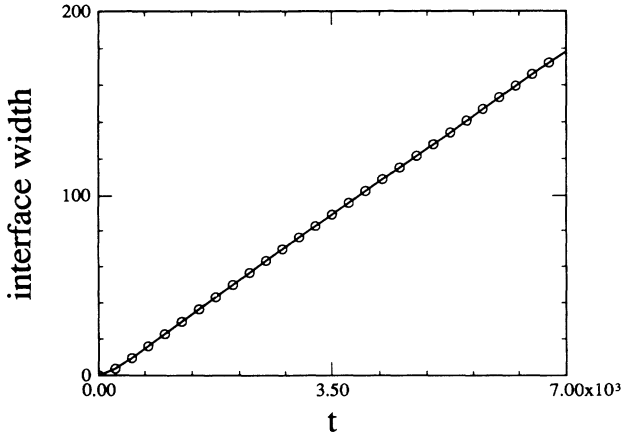

FIG. 8. Width of the interface, defined as the root-mean-square value of $\zeta(x)$, with $\epsilon = 0.4$ (solid line) and $\epsilon = 0.0$ (circles). Other parameters are the same as those of Fig. 3.

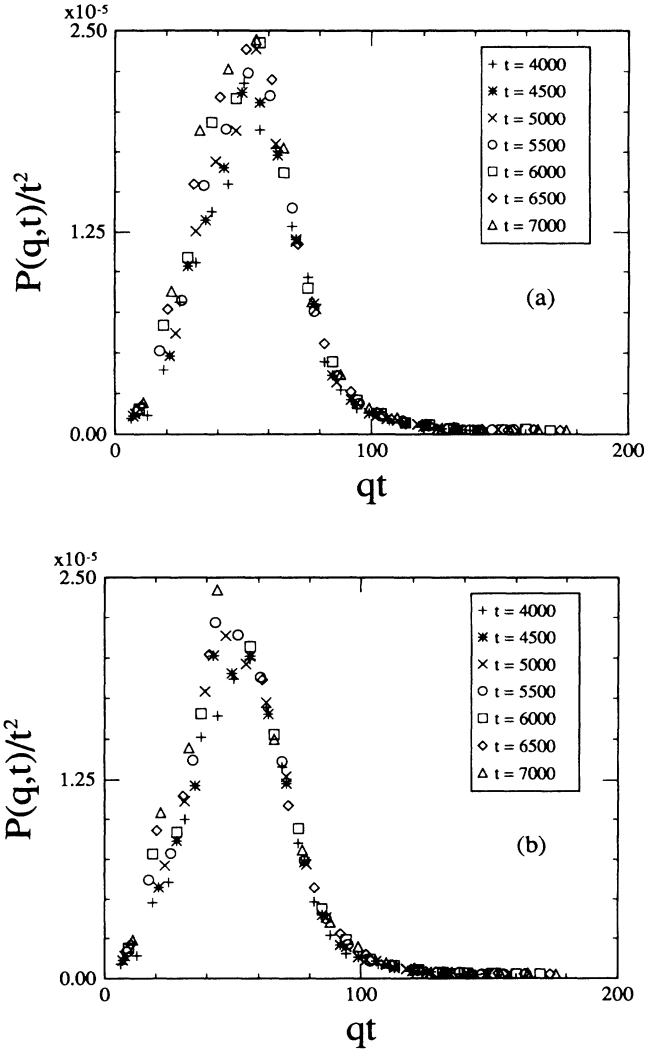

FIG. 9. Scaling function of (23) plotted for the case with $\epsilon \neq 0.4$. Other parameters are the same as those of Fig. 3. The data collapse reasonably well onto one curve, indicating that the perturbation of Eq. (24) does not change the scaling behavior of the transient dynamics. The data are a result of averaging 280 independent runs. (a) $\epsilon = 0.2$; (b) $\epsilon = 0.4$.

perturbation in (24) will be more important when the transient time regime is passed. This is definitely true in the steady-state limit [15]. Finally, we note that the scaling discussed here will eventually break down when the coarsening is nearly finished. The dynamics at this crossover regime can also be studied using the current numerical technique.

IV. SUMMARY

From the two models studied here, we may conclude that the long-wavelength dynamical behavior in the transient time regime has a generic feature that the power spectrum of the interface shape has a simple scaling form. For driven explosive crystallization, we were able to show this behavior analytically and obtained the scaling exponents. For the viscous-fingering problem, numerical techniques were employed. We have confirmed the findings of Ref. [12]. Furthermore, a local surface tension perturbation, which leads to a singular response in the steady-state pattern selection, does not seem to change the scaling behavior. While the two systems studied here belong to different universality classes, it is still not clear at this point what are the crucial factors that determine universality in systems far from equilibrium such as ours. It will be quite interesting to carry out a similar analysis for the dendritic growth.

The analytical method used here may be generalized to other more complicated pattern-forming systems and we are currently exploring this possibility. The numerical technique allows us to follow the evolving pattern from the very beginning to the final steady state. It is thus possible to study the crossover from the transient to such a steady state. This is important since we expect that the singular role played by the surface tension will be more visible in the crossover regime.

ACKNOWLEDGMENTS

H.G. thanks Dr. Jorge Viñals and Professor D. Jasnow for many useful discussions and generous help on the development of the numerical code. H.G. is supported by the Natural Sciences and Engineering Research Council of Canada, and le Fonds pour la Formation des Chercheurs et l'Aide à la Recherche de la Province du Québec. D.C.H. is supported by the Petroleum Research Fund administered by the American Chemical Society, and the Center for Polymer Science & Engineering, which is supported by NSF. Part of the computation has been conducted on the Cornell National Supercomputer Facility (CNSF). The CNSF is a resource of the Center for Theory and Simulation in Science and Engineering (Theory Center), which receives major funding from the NSF and IBM Corporation, with additional support from New York State and members of the Corporate Research Institute. The authors gratefully acknowledge the support.

[1] P.G. Saffman and G.I. Taylor, Proc. R. Soc. London, Ser. A **245**, 312 (1958); P.G. Saffman, J. Fluid Mech. **173**, 73 (1986); D. Bensimon, L. Kadanoff, S. Liang, B. Schraiman, and C. Tang, Rev. Mod. Phys. **58**, 977 (1986); G.M. Homsey, Ann. Rev. Fluid Mech. **19**, 271 (1987).

[2] J.S. Langer, in *Chance and Matter*, Proceedings of the Les Houches Summer School Session 46, edited by J. Souletie, J. Vannimenus, and R. Stora (North-Holland, Amsterdam, 1986).

[3] See, for example, articles included in *Dynamics of Curved Fronts*, edited by P. Pelcé (Academic, Boston, 1988).

[4] D. Kessler, J. Koplik, and H. Levine, Adv. Phys. **37**, 255 (1988).

[5] G.H. Gilmer and H.J. Leamy, in *Laser and Electron Beam Processing of Materials*, edited by C.W. White and P.S. Peercy (Academic, New York, 1980).

[6] W. van Saarloos, and J. D. Weeks, Phys. Rev. Lett. **51**, 1046 (1983); D.A. Kurtze, W. van Saarloos and J.D. Weeks, Phys. Rev. B **30**, 1398 (1984).

[7] C.P. Grigoropoulos , R.H. Buckholz, and G.A. Domoto, J. Appl. Phys. **52**, 454 (1986).

[8] B. Schraiman, Phys. Rev. Lett. **56**, 2028 (1986); D.C. Hong and J.S. Langer, *ibid.* **56**, 2032 (1986); R. Combescot, T. Dombre, V. Hakim, Y. Pomeau, and A. Pumir, *ibid.* **56**, 2036 (1986).

[9] D.A. Kurtze, Phys. Rev. Lett. **60**, 1683 (1988).

[10] W.W. Mullins and R.F. Sekerka, J. Appl. Phys. **34**, 323 (1963).

[11] See, for example, G. Barenblatt and Ya. B. Zeldovich, Ann. Rev. Fluid Mech. **4**, 285 (1972).

[12] D. Jasnow and J. Viñals, Phys. Rev. A **41**, 6910 (1990).

[13] D. Jasnow and J. Viñals (private communication).

[14] M. Rabaud, Y. Couder, and G. Gerard, Phys. Rev. A **35**, 1894 (1987); Z. Zocchi, B. Shaw, A. Libchaber, and L. Kadanoff, *ibid.* **36**, 1894 (1986).

[15] D.C. Hong and J.S. Langer, Phys. Rev. A **36**, 2325 (1986); D.C. Hong, *ibid.* **39**, 2042 (1989); H. Guo and D.C. Hong, *ibid.* **41**, 2995 (1990); R. Combescot and T. Dombre, *ibid.* **39**, 3525 (1989).

[16] R.B. Gold, J.F. Gibbons, T.J. Magee, J. Peng, R. Ormond, V.R. Deline, and C.A. Evans, in *Laser and Electron Beam Processing of Materials*, edited by C.W. White and P.S. Peercy (Academic, New York, 1980).

[17] S. A. Curtis and J. Maher, Phys. Rev. Lett. **63**, 2729 (1989).

[18] A different numerical technique is provided by G. Tryggvason and H. Aref, J. Fluid Mech. **136**, 1 (1983); **154**, 287 (1985).

[19] See, for example, the review of Bensimon *et al.* in Ref. [1].

[20] J. Viñals and D. Jasnow (unpublished).

[21] G.F. Miller, in *Numerical Solution of Integral Equations*, edited by L.M. Delves and J. Walsh (Clarendon, Oxford, 1974).

[22] M.A. Jaswon and G.T. Symm, *Integral Equation Methods in Potential Theory and Elastostatics* (Academic, New York, 1977), p. 129.

[23] We thank J. Viñals and D. Jasnow for pointing out to

us that reproducing the linear solution very accurately is actually a stringent test of the numerical code. See, also, Ref. [20].

[24] D. Kessler, J. Koplik, and H. Levine, Phys. Rev. A **30**, 2820 (1984).

[25] Numerical difficulty prevented us from reaching the steady state when too many modes were included in the initial curve. However, we were able to reach that state if fewer than 6 modes were included.

[26] As we have checked, for other values of n such as $n = 6$, the results were qualitatively the same.